400 equiv of 1-bromopropane. Before scanning in a negative direction, no oxidation waves are observed up to +0.9 V, which is the anodic limit of the solvent. However, after negatively scanning past the first reduction of $[(TPP)Rh(L)_2]^+Cl^-$ (wave 1), a new oxidation wave is observed at +0.34 V for 1-iodopropane (wave 5, Figure 7a) and at +0.73 V for 1-bromopropane (wave 6, Figure 7b). $(TPP)Rh(C_5H_{11})$ is formed in both cases and is not oxidized until potentials more positive than +1.0 V. Similar cyclic voltammetric results were obtained with all of the RI and RBr compounds which showed reactivity (see Table I). Cyclic voltammetric experiments show that tetrabutylammonium iodide (TBAI) and tetrabutylammonium bromide (TBABr) are irreversibly oxidized at +0.34 and +0.73 V, respectively (see Figure 7c,d). Thus the wave at +0.34 V in Figure 7a is assigned as the oxidation of I^- and the wave at +0.73 V in Figure 7b as the oxidation of Br^-. These potentials agree with potentials given in previous reports[29] for the oxidation of I^- and Br^-.

Integration of the total current for the first reduction peak of $[(TPP)Rh(L)_2]^+Cl^-$ in the presence of RX gives coulometric values of n that are dependent upon RX. When X = Cl, $n = 1.0 \pm 0.1$ electron per Rh atom. In contrast, when X = Br and I, $n = 1.3 \pm 0.1$ and 1.5 ± 0.1 electron per Rh atom, respectively. Formation of (TPP)Rh(R) and Cl^- from $[(TPP)Rh(L)_2]^+$ and RCl requires a total of two electrons, and this is not experimentally observed. Thus the overall reaction for formation of (TPP)Rh(R) can best be described by equations 1-3, where S is an electron source other than the electrode.

$$[(TPP)Rh(L)_2]^+ \xrightarrow{e} (TPP)Rh + 2L \quad (1)$$

$$(TPP)Rh + RX \rightarrow (TPP)Rh(R) + X^\bullet \quad (2a)$$

$$(TPP)Rh + RX \rightarrow [(TPP)Rh(R)]^+ + X^- \quad (2b)$$

$$X^\bullet + S \rightarrow X^- + S^+ \quad (3a)$$

$$[(TPP)Rh(R)]^+ + S \rightarrow (TPP)Rh(R) + S^+ \quad (3b)$$

After generation of (TPP)Rh and attack at the R-X bond, either loss of $X^\bullet$ and formation of (TPP)Rh(R) (eq 2a) or loss of X^- and formation of $[(TPP)Rh(R)]^+$ (eq 2b) will occur. Reaction pathways 2a and 3a will be followed when X = Br and I. In this case $X^\bullet$ formation can occur if one considers that the potential for the $(TPP)Rh(R)/[(TPP)Rh(R)]^+$ couple is near +1.0 V in benzonitrile,[30] while the $X^-/X^\bullet$ potential is less than +1.0 V. On the other hand, path 2b and 3b will be followed when X = Cl or F. The $X^-/X^\bullet$ potential of chloride and fluoride is greater than 1.0 V, and reaction paths 2a and 3a will not occur. However, in the case of X = Br and I, some electrochemical reduction of $X^\bullet$ to X^- is observed thus accounting for the increase in coulometric value of n. Apparently, some $I^\bullet$ and $Br^\bullet$ have time to diffuse back to the electrode surface after the chemical reaction between RX and (TPP)Rh. It should be noted that a careful measurement of the background current was performed in the presence of RX and the possibility that the increase in n for X = Br and X = I was due to direct reduction of RX was eliminated.

Formation of (TPP)RhX is not observed in any of the electrochemical or spectroelectrochemical experiments. For example, (TPP)RhCl is reduced at -1.2 V in benzonitrile,[30] and the generation of this species would be observed by the cyclic voltammograms. This lack of (TPP)RhX generation is in contrast to reports that the reaction of $[(P)Rh]_2$ with RX gives (P)Rh(X).[3,5,12]

A mechanism has been previously proposed for the reaction of $[(OEP)Rh]_2$ with RX.[12] (OEP)Rh is proposed to react with RX to form (P)Rh(X) and $R^\bullet$ after dissociation of the dimer. The $R^\bullet$ radical then combines with another $[(OEP)Rh]_2$ unit to form (OEP)Rh(R). The data presented in this paper clearly suggests an alternate pathway for the reaction of (TPP)Rh and RX as indicated by eq 1-3. The effects of R and X on the overall rate constant are consistent with this type of reaction pathway and not with $R^\bullet$ formation. However, the observation of different reaction pathways and different products in these two studies can be rationalized if one considers the relative stabilities of $R^\bullet$. In the present case, formation of $R^\bullet$ would result in generation of a radical such as $CH_3^\bullet$ or $(C_nH_{2n+1})^\bullet$. In the previous study formation of $C_6H_5CH_2^\bullet$ was proposed, which is considerably more stable.[28] Hence, in the latter case a radical pathway may predominate.

Acknowledgment. The support of the National Science Foundation (Grant No. CHE-8515411) is gratefully acknowledged.

(29) Bard, A. J.; Merz, A. *J. Am. Chem. Soc.* **1979**, *101*, 2959.

(30) Unpublished data.

A Comparison of Electron Donor and Proton Abstraction Activities of Thermally Activated Pure Magnesium Oxide and Doped Magnesium Oxides

Kenneth J. Klabunde* and Hiromi Matsuhashi

Contribution from the Department of Chemistry, Kansas State University, Manhattan, Kansas 66506. *Received June 30, 1986*

Abstract: Thermal activation of microcrystalline MgO at 400-700 °C has been carried out under vacuum and under rapid flows of N_2, Ar, O_2, and H_2/N_2. Some samples of MgO were impregnated or coprecipitated with LiOH, NaOH, or $Al(OH)_3$ before activation. The activities for 1-butene isomerization, where proton abstraction is rate limiting, were compared with activities for CO telomerization/reduction, where electron donation capability is most important. These studies suggest that defect sites are involved and that localized electron rich domains can be enhanced by Li^+ substitution for Mg^{2+} but that localized more electron difficient domains can be enhanced by Al^{3+} substitution for Mg^{2+}. These studies also show that high-temperature thermal activation with gas flow of N_2 or Ar is possible, but that O_2 and H_2/N_2 anneal out defects and activity is lost.

The remarkable properties of thermally activated polycrystalline MgO are well-documented.[1] To illustrate this consider the following: (1) catalysis of $H_2 + D_2 \rightarrow 2HD$, $E_a \sim 2$ kcal/mol which is considerably lower than the gas-phase E_a for $H^\bullet + D_2$

0002-7863/87/1509-1111$01.50/0

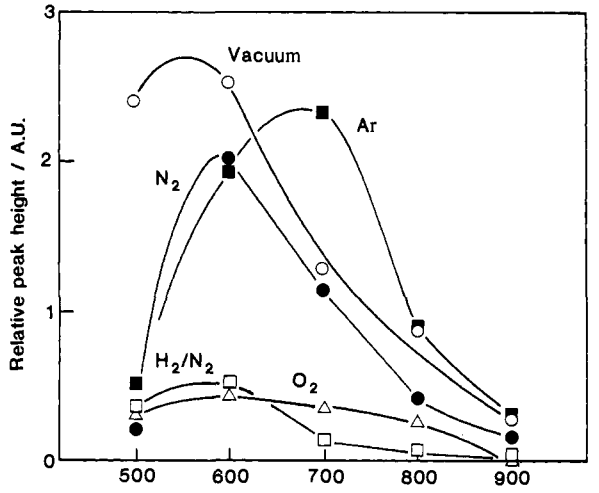

Figure 1. Relative peak height (arbitrary units) vs. thermal activation temperature °C.

Table I. Effect of N_2 Gas Flow on Activity of MgO for CO Radical Formation[a]

flow rate (mL/min)	reactive activity[b]
50	1.27
100	1.20
200	2.00
300	2.50

[a] Sample weight = 35 mg of MgO; activation temperature = 600 °C; CO pressure = 150 torr (20 kPa) for 1 week. [b] ESR signal for $(CO)_6^{\bullet 3-}$ measured relative to Mn^{2+} impurity line.

→ HD + D•;[2] (2) $ArCH_3 + D_2 \rightarrow ArCH_2D + HD$, $E_a \sim 1$ kcal/mol;[3] (3) CO is telomerized and reduced to $(CO)_n^{x-}$, especially $(CO)_2^{2-}$ and $(CO)_6^{\bullet 3-}$ at room temperature and below;[4] (4) organophosphorus compounds are decomposed stoichiometrically under mild conditions;[5] (5) alkenes are catalytically isomerized at 0 °C;[6] and (6) dienes are catalytically deuteriated at 0 °C without scrambling.[7] And there are other examples of equally surprising behavior, including methane activation.[8]

The high activity of such an ionic, insulator oxide is apparently due to, in addition to basic sites, surface defects that are formed during oxide preparation and activation that persist even at elevated temperatures.[9] When these sites are freed of adsorbed H_2O, CO_2, and many OH groups, they possess extremely basic properties as well as electron donor properties.[10]

The current study was carried out so that two well-known reactions on activated MgO could be compared and monitored while the surface properties of MgO were changed by (a) activation temperature (vacuum), (b) activation with high temperature gases N_2, Ar, O_2; and H_2/N_2, and (c) doping with Li, Na, and Al oxides/hydroxide. The probe reactions chosen were 1-butene isomerization, where proton abstraction is rate-limiting,[6] and CO telomerization reduction to $(CO)_n^{x-}$ where electron donor properties are most important.[4]

(1) *Adsorption and Catalysis on Oxide Surfaces*; Che, M.; Bond, G. C., Eds.; Studies in Surface Science and Catalysis 21; Elsevier: Amsterdam, 1985.
(2) Boudart, M.; Delbouille, A.; Derouane, E. G.; Indovina, V.; Walters, A. B. *J. Am. Chem. Soc.* **1972**, *94*, 6622–6630.
(3) Hoq, M. F.; Klabunde, K. J. *J. Am. Chem. Soc.* **1986**, *108*, 2114–2116.
(4) Morris, R.; Klabunde, K. J. *J. Am. Chem. Soc.* **1983**, *105*, 2633–2639.
(5) Lin, S. T.; Klabunde, K. J. *Langmuir* **1985**, *1*, 600–605.
(6) (a) Kijenski, J.; Malinowski, S. *J. Chem. Soc., Faraday Trans. 1* **1978**, *74*, 250. (b) Matuda, T.; Tanabe, K.; Hayashi, N.; Sasaki, Y.; Miura, H.; Sugiyama, K. *Bull. Chem. Soc. Jpn.* **1982**, *55*, 990. (c) Hattori, H.; Shimazu, K.; Yoshii, N.; Tanabe, K. *Bull. Chem. Soc. Jpn.* **1976**, *49*, 969.
(7) Hattori, H.; Tanaka, Y.; Tanabe, K. *J. Am. Chem. Soc.* **1976**, *98*, 4652.
(8) Driscoll, D.; Martir, W.; Wang, J.; Lunsford, J. *J. Am. Chem. Soc.* **1985**, *107*, 58 have studied M_3O and Li doped MgO in methane activation catalysis.
(9) Morris, R.; Klabunde, K. J. *Inorg. Chem.* **1983**, *22*, 682–687.
(10) Tanabe, K. *Solid Acids and Bases*; Academic: New York, 1970.

Table II. Surface Areas of Some MgO Samples

activtn temp (°C)	MgO	MgO-p	MgO-Na-i
400	213	188	128
500	139	167	93
600	140	128	82
700	130	108	88

Table III. 1-Butene Isomerization Rates (cis/trans Ratios) on MgO and Mixed Oxide Catalysts[a,b]

	activation temperatures[c] (°C)			
catalyst[c]	400	500	600	700
MgO	2.68 (5.33)	3.01 (4.68)	0.98 (5.95)	0.11 (9.71)
MgO-p	1.88 (6.77)	2.81 (6.71)	1.25 (5.33)	0.29 (10.01)
MgO-Na	1.48 (5.10)	3.09 (4.62)	2.01 (4.40)	0.60 (4.37)
MgO-Li	1.03 (5.49)	1.67 (4.93)	0.44 (5.00)	0.24 (2.95)
MgO-Al-i	12.0 (2.68)	10.4 (4.03)	3.97 (4.65)	0.70 (3.14)
MgO-Al-p	3.23 (8.58)	1.48 (9.68)	0.73 (8.81)	0.08 (8.53)

[a] Reaction rate, $\times 10^{21}$ molecules-g^{-1}-min^{-1} (data taken at nearly constant conversions; first order in 1-butene). [b] Reaction conditions: 1-butene pressure = 100 torr, reaction temperature = 0 °C. [c] See text and Experimental Section for preparative conditions.

Results

A. Activation Temperature. Four temperatures were chosen: 400, 500, 600, and 700 °C. Vacuum activation was done slowly over 3 h with good pumping speed so that H_2O given off was rapidly pumped away. It is known that undesirably high H_2O vapor pressures can cause sintering of MgO surface features.

B. Treatment with High-Temperature Gases. We first needed to demonstrate that MgO activation could be carried out under a flow of inert gas. We used the CO → $(CO)_6^{\bullet 3-}$ reaction as a probe of surface activity.[4] Figure 1 plots activity vs. activation temperature of N_2, Ar, O_2, and H_2/N_2 gases, which demonstrates that flowing N_2 or Ar allow MgO activation almost as well as vacuum. However, only small samples could be activated in this way, and the flow rate was a critical parameter (Table I). Larger samples required faster flow rates to carry the generated steam off quickly. We were unable to obtain active MgO when 50 g were thermally treated at 600 °C with a N_2 flow approaching 1000 mL/min. Thus, for large samples vacuum activation is preferable unless very high gas flow rates can be employed (preheating of the gas is necessary under such high flow conditions). Figure 1 also illustrates the effects of using O_2 and 10% H_2/N_2 for high temperature gas flow activation. Note that in both cases electron donor capabilities were severely retarded.

In all of these experiments a short evacuation time (5 min) at activation temperature was necessary as a last step in order to remove adsorbed molecules of flow gas. This also ensured that the final surfaces were cleaned of peroxide or hydroxide groups that were present due to the presence of hot O_2 or H_2.

C. Doping with Li, Na, and Al Oxides/Hydroxides. Active MgO was prepared by boiling commercial high purity MgO in water followed by drying and thermal treatment (MgO) or by precipitating $Mg(OH)_2$ by using the reaction $Mg(NO_3) + NH_4OH \rightarrow Mg(OH)_2 + NH_4NO_3$ followed by washing, drying, and thermal activation (MgO-p).

Slurried $MgO/Mg(OH)_2$ was impregnated with NaOH and LiOH in water solution, the water was evaporated, and the solid was dried and thermally treated (MgO–Na, MgO–Li). In the case of Al, MgO slurried in EtOH was treated with a solution of $Al[OCH(CH_3)_2]_3$ in ethanol, water was added, and the resultant $Al(OH)_3$ impregnated the MgO. Filtration, washing, drying, and thermal treatment followed (MgO–Al–i). A second method was used, that of coprecipitation. $Mg(NO_3)_2$ and $Al(NO_3)_3$ were dissolved in water and coprecipitated as hydroxide by addition of NH_4OH solution. Filtration, drying, and thermal treatment followed.

Surface areas for several MgO samples are listed in Table II.

1-Butene Isomerization. Table III summarizes the activities of these catalysts for 1-butene isomerization. Note that 500 °C

Table IV. CO Radical Formation on MgO and Mixed Oxide Catalysts[a,b]

catalyst	activation temperatures (°C)			
	400	500	600	700
MgO	0.29	2.10	4.23	2.62
MgO-p	0.42	2.91	4.37	3.27
MgO-Na-i	0.26	2.37	4.37	1.98
MgO-Li-i	0.50	1.85	5.24	2.11
MgO-Al-i	0.26	0.34	0.91	1.70
MgO-Al-p	0.04	0.21	0.28	0.26

[a] Relative intensity of ESR peak for $(CO)_6^{\bullet 3-}$ vs. Mn^{2+} impurity peak. [b] CO initial pressure: 150 torr (20 kPa), adsorbed for one week at room temperature.

activation was best for both pure MgO samples, MgO–Na and MgO–Li. The lowest activation temperature was best for the MgO–Al-i and MgO–Al-p. Also note that the overall activity was nearly unchanged by Na^+, decreased slightly by Li^+, and increased dramatically by Al^{3+} addition. Cis/trans ratios were also varied and are shown in Table III. The most striking finding is that MgO–Al-i showed greatly increased activity, lower required activation temperature, and a lower cis/trans ratio.

CO Radical Formation. Table IV summarizes the data of the mixed oxide's ability to donate electrons and form $(CO)_6^{\bullet 3-}$.[4] It appears that Na^+ addition had little effect. On the other hand, Li^+ addition had a moderate beneficial effect. And most interesting, Al^{3+} addition caused a dramatic lowering in activity.

Discussion

Effects of High-Temperature O_2 or H_2. High-temperature O_2 and H_2 both cause dramatic decreases in MgO electron donor properties. Both gases could have a tendency to anneal out defects. For example O_2 may provide O^{2-} for satisfying anion vacancies and excess O^{2-} in the nearby lattice taken up to reform O_2. Similarly, O_2 may oxidize cation vacancies creating a hole that may migrate and encourage Mg^{2+} migration to the cation vacancy area. Analogously, H_2 may provide H^- for anion vacancies (temporarily) and H^+ for cation vacancies. Reformation of H_2 could cause surface restructuring in the process. It seems that the most likely explanation is an annealling effect of H_2 and O_2 to yield a less defective surface.

The preparative methods used for Na^+ and Li^+ impregnation would suggest that a significant amount of the surface cations would be Na^+ or Li^+ (a 5 % loading overall, but surface impregnation might lead to as high as 50 % of the surface cations being Na^+ or Li^+). And yet no substantial effects on 1-butene isomerization or CO radical formation were noted with Na^+. However, Li^+ did cause a moderate decrease in activity for 1-butene isomerization and a moderate increase in activity for CO radical formation (at the optimum activation temperatures). It might be expected that Li^+ (ionic radius = 0.68) would more readily be adsorbed into the MgO lattice (Mg^{2+} ionic radius = 0.66), whereas Na^+ may not (Na^+ ionic radius = 0.97).

The effects of Al^{3+} impregnation were dramatic showing a large increase in 1-butene isomerization along with a lowering of optimum activation temperature. Conversely, Al^{3+} impregnation caused a severe retardation in the CO radical formation process.

It seems that we can be certain of at least two things: (1) Active sites for 1-butene isomerization and CO radical formation are different. This we can deduce from the different optimum activation temperatures and the opposing effects of Li^+ vs. Al^{3+} impregnation. (2) These different sites can be poisoned or enhanced by properly selected doping procedures. Indeed these materials exhibit unique properties and Li^+ and Al^{3+} can be considered promotors or poisons. It should be stressed that pure, activated MgO and pure, activated Al_2O_3 do not mimic these doped samples.[11]

Lower activation temperatures are optimum for 1-butene isomerization, usually 500 °C. Most dehydration and surface reconstruction occurs in the 400–500 °C range. Surface areas are highest after 400 °C treatment, but near complete dehydration is reached at 500 °C. It could be concluded that the highest surface with a high-surface density of defects is best for 1-butene isomerization. However, even more "highly defective" sites are needed for CO radical formation, and in order to reveal these sites, even higher activation temperatures are needed. Thus, it is the types of sites available and not the number of sites (surface area) that is important for this reaction.[4,9]

Following the work of Coluccia and Tench,[12] Hattori[13] has proposed that there are three sites S_I, S_{II}, and S_{III} progressively revealed by higher activation temperatures. Structural defects (corners, edges) allow O^{2-}_{LC} and Mg^{2+}_{LC} (LC = lower coordination) to exist. Coordinative unsaturation is greatest for $Mg^{2+}_{3C}O^{2-}_{3C}$, so he proposes this formulation for the S_{III} sites which can only be revealed at activation temperatures >700 °C. S_{II} may be $3Mg^{2+}_{3C}O^{2-}_{4C}$ sites which are active for H–D exchange and amination (activation temperature 600–700 °C). Our work would suggest S_{II} sites are also active in electron donation. S_I sites are active for isomerization and are revealed at activation temperatures of 400–600 °C. S_I may be edge sites such as $Mg^{2+}_{4C}O^{2-}_{4C}$.

Expanding on the structural defect idea, if an edge site were doped with Li we could envision a partial crystallite (with or without long range order) as

$$\begin{bmatrix} Li & O & Mg & O & Li & O \\ O & Mg & O & Li & O & Mg \\ Mg & O & Mg & O & Mg & O \end{bmatrix}^{3-}$$

Due to Li^+ substituting for Mg^{2+}, this small surface piece would bear a charge as $[Li_3Mg_6O_9]^{3-}$. Other parts of the bulk would possess anion vacancies for charge balance.

If we assume that this negative charge is localized over a small portion of the crystallite, say a $Li_3Mg_6O_9^{3-}$ portion, this might serve as a source of electrons for donation to CO

$$[Li_3Mg_6O_9]^{3-} + 7CO \rightarrow Li_3Mg_6CO_{10} + C_6O_6^{\bullet 3-}$$

In other words, one CO is oxidized to carbonate releasing electrons for telomerization/electron reduction of 6CO.[14] Analogous reasoning for formation of $C_6O_6^{2-}$ can be used if a piece of the crystallite is richer in Mg^{2+}

$$[Li_2Mg_7O_9]^{2-} + 7CO \rightarrow Li_2Mg_7CO_{10} + C_6O_6^{2-}$$

Anion vacancies may serve as sites for adsorption of the $(CO)_n^{x-}$ species.

This reasoning can be used to explain Li^+ doping aiding electron donation properties. To explain its modest retardation of 1-butene isomerization activity, we may use similar reasoning. A $[Li_3Mg_6O_9]^{3-}$ or $[Li_2Mg_7O_9]^{2-}$ or similar moiety would probably serve as a good area for H^+ abstraction, but a poor area for stabilization of the resultant allyl anion

$$[Li_3Mg_6O_9]^{3-} + H_2C{=}CHCH_2CH_3 \rightarrow [Li_3Mg_6O_9H]^{2-}[CH_2{=}CHCHCH_3]^-$$

Therefore, the E_a for formation of the allyl anion may be higher. This leads us to consider Al^{3+} doping.

If a similar crystallite portion is illustrated with Al^{3+} doping we have $[Al_3Mg_6O_9]^{3+}$

$$\begin{bmatrix} Al & O & Mg & O & Al & O \\ O & Mg & O & Al & O & Mg \\ Mg & O & Mg & O & Mg & O \end{bmatrix}^{3+}$$

Cation vacancies in the bulk would be present to equalize charge. A moiety like $[Al_3Mg_6O_9]^{3+}$ would have very poor electron donor properties, and thus Al^{3+} doping would have the effect of drastically curtailing $C_6O_6^{\bullet 3-}$ production. On the other hand, a moiety like $[Al_3Mg_6O_9]^{3+}$ would be quite effective at stabilizing an allyl anion, thus perhaps lowering the barrier for 1-butene isomerization.

(11) Klabunde, K. J.; Kaba, R. A.; Morris, R. M. *Inorganic Compounds with Unusual Properties II*; Advances in Chemistry Series 173; American Chemical Society: Washington, DC, 1979; p 140–151.

(12) Coluccia, S.; Tench, A. J. *Proc. 7th Int. Cong. Catal.* **1980**, p 1160.

(13) Hattori, H., in ref 1, pp 319–330.

(14) IR has shown that carbonate is formed: Morris, R. M.; Kaba, R. A., Groshens, T. J.; Klabunde, K. J.; Baltisberger, R. J.; Woolsey, N. F.; Stenberg, V. I. *J. Am. Chem. Soc.* **1980**, *102*, 3419–3424.

Thus, base sites would still be involved in H^+ abstraction, but the resultant allyl anion would bind strongly to the $[Al_3Mg_6O_9]^{3+}$ site. The fact that the most active catalyst (MgO–Al-i) yields a lower cis/trans ratio[6] is probably due to secondary cis→trans isomerization.

Another possibility is that the presence of Al^{3+} yields surface sites that can catalyze 1-butene isomerization in an acidic manner (proton donation rather than proton abstraction). We believe this is rather unlikely since we have also shown these Al^{3+} doped catalysts to be active in $RH + D_2 \rightarrow RD + HD$ catalysis, which is definitely induced by basic sites.[15]

Conclusions

(1) Surface defects are responsible for 1-butene isomerization and CO radical formation. However, different types of sites are necessary for each process. Surface domains of varying electron density seem to play a role.

(2) High-temperature O_2 and H_2 anneal out many surface defects.

(3) Gas flow activation using N_2 or Ar can be employed for MgO thermal activation, although vacuum activation remains preferrable for large samples.

(4) Na^+ doping has little effect on 1-butene isomerization or CO radical formation (electron donor properties).

(5) Li^+ doping retards 1-butene isomerization, but aids CO radical formation. The presence of Li^+ in the surface lattice causes an increase in electron donation ability.

(6) Al^{3+} doping greatly increases 1-butene isomerization ability through the creation of moieties that can better stabilize intermediate allyl anions (more Lewis acidic surface). Likewise, these more acidic moieties drastically retard electron donation properties and thus retard CO radical formation ($CO \rightarrow (CO)_6^{\bullet 3-}$).

Experimental Section

Preparation of Oxides. MgO. Pure, anhydrous MgO (ROC/RIC ultrapure 99.999%) was treated with boiling distilled water to hydroxylate the surface, followed by drying and thermal activation. For example, 10 g was placed in a beaker and boiled for 1 h with 300 mL of distilled water. The while solid was filtered off and dried in an oven at 100 °C for 12 h. Then 0.1 g was placed in a quartz U-tube with a piece of glass wool placed near the top of each side. Thermal activation was carried out in two ways: (1) Vacuum; the sample was pumped down to $\times 10^{-6}$ torr and slowly heated (2 h) to the desired activation temperature and held for 3 h, followed by slow cooling to room temperature (2 h). Pumping was maintained during the entire manipulation. (2) *Gas flow*; the gases used were high purity. N_2 was passed through a 100-°C deoxygenation catalyst and then a −196-°C trap. H_2/N_2 was passed through a −196-°C trap, and Ar and O_2 were passed through a cold ethanol trap (<−120 °C). About 50 mg of $Mg(OH)_2$/MgO (from boiling MgO in distilled water) was placed in a quartz U-tube (8-mm ID, 20-cm long) and held in place with glass wool. The air was purged by evacuation, then the desired gas flow was started, and the sample was slowly heated (2 h) to the desired activation temperature and held for 3 h, followed by a 5-min evacuation time and then slow cool down (2 h).

MgO-p. $Mg(NO_3)_2 \cdot 6H_2O$ (130 g) (MCB Reagents) was dissolved in 600 mL of distilled water, and then 35 mL of a 26% aqueous NH_3 solution (Fisher Scientific) was added with stirring. A white precipitate formed and was collected by filtration. The solid was washed with 600 mL of distilled water, crushed, and dried in air at 500 °C for 1 h. It was cooled, then boiled in distilled water for 1 h, filtered, and dried in a 100-°C oven overnight. Portions were thermally activated as needed.

MgO–Na, MgO–Li. MgO powder (10 g) (ROC/RIC ultrapure) was placed in 300 mL of boiling distilled water for 0.5 h. Then 0.5479 g of $LiOH \cdot H_2O$ (Aldrich) or 0.5222 g of NaOH (MCB Reagent) was dissolved in 100 mL of distilled water and heated to boiling. The two boiling solutions were mixed and boiled for 1 h followed by water evaporation. The resulting solid was dried in an oven (120 °C) overnight. The Li^+ and Na^+ contents were 5.12 and 5.09 atomic % respectively (atomic absorption analysis). Portions were thermally activated as needed.

MgO–Al-i. MgO powder (10 g) (ROC/RIC ultrapure) was placed in 300 mL of ethanol with stirring. Then 25 g of $Al[OCH(CH_3)_2]_3$ (Aldrich) was slowly added with stirring. Then 300 mL of distilled, deionized water was added, which decomposed the aluminum isopropoxide to $Al(OH)_3$ which is not water soluble. The water/ethanol was evaporated, and the dry solid was boiled in 300 mL of distilled water for 1 h. The white solid was filtered and dried in an oven (120 °C) overnight. The Al content was 4.80 atomic % (atomic absorption).

MgO–Al-p. $Mg(NO_3)_2 \cdot 6H_2O$ (128 g) and $Al(NO_3)_3 \cdot 9H_2O$ (9.88 g) (Fisher) were dissolved in distilled water (total volume = 300 mL). Then 35 mL of a 26 % aqueous NH_3 solution (Fisher) was added with stirring. The resulting white precipitate was filtered off and dried in an oven overnight (120 °C). The solid was placed in 300 mL of boiling distilled water, boiled for 1 h, filtered, and dried again in the oven. The Al content was 5.01 atomic %. Portions were thermally activated as needed.

Measurement of CO Radical Formation Activity[4] ($CO \rightarrow C_6O_6^{\bullet 3-}$). The thermally activated sample was cooled to room temperature and 100 mg was placed in a quartz ESR tube. Then 150 torr of CO was placed over the sample, and it was allowed to stand for exactly 1 week. The color changed from white to yellow-pink. An ESR spectrum was recorded and compared to the peak height of a Mn^{2+} impurity line (3263 G) (a common MgO sample was used for all work except MgO-p and MgO–Al-p). In the case of the coprecipitated samples MgO-p and Mg–Al-p the Mn^{2+} impurity line was normalized to that in the common MgO sample.

1-Butene Isomerization. A 10–50-mg sample was thermally activated in a flow reactor. It was cooled to 0 °C; and 1-butene flowed over it as previously described by Tanabe and co-workers.[6] The pressure of starting 1-butene was 100 torr. Samples were extracted for GC analysis periodically.

Acknowledgment. The support of the Army Research Office (Grant DAAG29-84-K-0051) is acknowledged with gratitude.

Registry No. MgO, 1309-48-4; Li, 7439-93-2; Na, 7440-23-5; Al, 7429-90-5; H^+, 12408-02-5.

(15) Hoq, M. F., unpublished results from this laboratory.